

**THE EFFECT OF RARE-EARTH SUBSTITUTION ON THE PROPERTIES  
OF BISMUTH TITANATE PREPARED BY LOW TEMPERATURE  
COMBUSTION TECHNIQUE**

**by**

**UMAR AL-AMANI BIN HAJI AZLAN**

**Thesis submitted in fulfillment of the requirements  
for the degree of  
Doctor of Philosophy**

**2013**

## ACKNOWLEDGEMENTS

First of foremost, I express my thanks to School of Material & Mineral Resources Engineering, USM for granting me the opportunity to further my PhD. Sincere gratitude to all my supervisors, Assoc. Prof. Dr. Srimala Sreekantan, Professor Ahmad Fauzi Mohd Noor and Assoc. Prof. Dr. Khairunisak Abd. Razak, for their invaluable guidance, support and encouragement in the realization of this work.

I would like to thank Professor Uematsu Keizo and Assoc. Prof. Dr. Satoshi Tanaka (Nagaoka University of Technology, Japan) for all of their kind helps and generous sharing with dielectric and ferroelectric measurements and Assoc. Prof. Dr. Naratip Vittayakorn (King Mongkut's Institute of Technology Ladkrabang, Thailand) for his help with ferroelectric measurement.

I also wish to thank USM and UTEM, for financial support. Thanks to all the academic and technical staffs in the School of Material & Mineral Resources Engineering, USM especially Professor Radzali Othman and Professor Azizan Aziz for their continual supports and assistance to finish this research. Many thanks goes to all of the group members in USM, particularly, my senior; Dr. Aye Aye Thant, for teaching me helpful combustion synthesis in the lab; Warapong @ Tony, Nazida, Dr. Suriati, Syahriza, Farah, Azlila, Hamisah, Hasmizam, Kee, Dr. Uday and Dr. Nilar for being great friends.

Finally, thanks to my beloved parents, the late Hj. Azlan Hj. Mohd Salleh and Hjh. Noor Aminah Ali Hanapiah. Thanks also to my parent-in-law, Mat Yusof Thalimon and Hatipah Abas. To my lovely wife, Malihah Mat Yusof and my kids, Nur Aina Umairah and Nur Auni Mawaddah, for all the love and sacrifice to me. This thesis is dedicated for them.

## TABLE OF CONTENTS

ACKNOWLEDGEMENTS .....	ii
TABLE OF CONTENTS .....	iii
LIST OF TABLE .....	viii
LIST OF FIGURE.....	ix
LIST OF ABBREVIATIONS.....	xiv
LIST OF SYMBOLS .....	xv
ABSTRAK .....	xvi
ABSTRACT.....	xviii
CHAPTER 1 .....	1
1.1    Research background.....	1
1.2    Problem statement .....	6
1.3    Research objectives .....	7
1.4    Scope of research.....	7
CHAPTER 2 .....	9
2.1    Introduction .....	9
2.2    General concept of functional materials.....	9
2.2.1    Structural origin of the ferroelectric state .....	12
2.3    Development of ferroelectric materials .....	13
2.3.1    Ferroelectric ceramic materials.....	14
2.3.2    Bismuth-layer structures .....	15
2.4    Bismuth titanate.....	16
2.4.1    Properties of BIT ceramics .....	17
2.4.1.1    Powder morphology .....	18
2.4.1.2    Grain microstructures .....	22
2.4.1.3    Dielectric and ferroelectric properties .....	23
2.4.2    Properties of thin/thick BIT films.....	25
2.4.3    Substitution in Bismuth titanate .....	28
2.4.3.1    Substitution on A-site .....	29
2.4.3.2    Substitution on B-site .....	37
2.4.3.3    Co-substitution on A- and B-sites .....	39
2.5    Method and processing routes .....	41
2.5.1    Mechanical activation technique .....	42
2.5.2    Sol-gel synthesis .....	44

2.5.3	Precipitation method.....	46
2.5.4	Hydrothermal synthesis .....	47
2.6	Combustion synthesis.....	49
2.6.1	Conventional SHS .....	50
2.6.2	Solution combustion synthesis .....	51
2.6.3	Critical factor in combustion synthesis.....	53
2.6.3.1	Nature of fuel.....	54
2.6.3.2	Ratio of fuel to oxidizer.....	56
2.7	Functional material applications.....	57
2.7.1	Memory technology.....	57
2.7.1.1	Static random access memory .....	59
2.7.1.2	Dynamic random access memory.....	59
2.7.1.3	Ferroelectric random access memory.....	61
2.8	Summary.....	62
CHAPTER 3 .....		63
3.1	Introduction .....	63
3.2	Raw materials .....	63
3.3	Experimental design .....	64
3.4	Powder preparation.....	66
3.4.1	Sol-gel auto combustion .....	66
3.4.2	Precipitation assisted low-temperature combustion .....	68
3.4.3	Synthesis of rare-earth substitution .....	69
3.5	Ceramic fabrication .....	71
3.5.1	Compaction.....	71
3.5.2	Sintering.....	72
3.6	Parameter studies.....	73
3.6.1	Effect of Ti excess .....	73
3.6.2	Effect of calcination temperature.....	73
3.6.3	Effect of sintering temperature .....	74
3.6.4	Effect of pH .....	74
3.6.5	Effect of hydrolysis temperature .....	75
3.6.6	Effect of rare-earth substitution.....	75
3.7	Characterization and measurement.....	76
3.7.1	X-Ray Diffraction.....	77

3.7.2	Field Emission Scanning Electron Microscopy.....	78
3.7.3	Raman spectroscopy .....	79
3.7.4	Photoluminescence spectroscopy .....	79
3.7.5	Fourier transform infrared spectroscopy analysis.....	79
3.7.6	Thermogravimetry-Differential thermal analysis .....	80
3.7.7	Transmission Electron Microscopy .....	80
3.7.8	Brunauer, Emmett and Teller analysis.....	81
3.7.9	Dilatometry analysis .....	81
3.7.10	Bulk density-porosity .....	81
3.7.11	X-ray photoelectron spectroscopy .....	82
3.7.12	Dielectric properties.....	83
3.7.13	Ferroelectric properties .....	84
CHAPTER 4 .....		86
4.1	Introduction .....	86
4.2	Synthesis I: Preparation of BIT bulk samples by SGAC .....	86
4.2.1	TG-DTA .....	86
4.2.2	Effect of Ti excess .....	88
4.2.2.1	XRD analysis.....	88
4.2.2.2	Raman analysis.....	91
4.2.2.3	FTIR analysis.....	94
4.2.2.4	Particle morphology .....	96
4.2.3	Effect of calcination temperature.....	97
4.2.3.1	XRD analysis.....	98
4.2.3.2	Particle morphology .....	102
4.2.3.3	TEM analysis.....	104
4.2.4	Effect of sintering temperature .....	105
4.2.4.1	Phase stability and grain orientation.....	105
4.2.4.2	Microstructure observation of sintered samples.....	107
4.2.4.3	Relative density- apparent porosity .....	109
4.2.4.4	Dielectric properties .....	110
4.2.4.5	Ferroelectric properties.....	112
4.2.5	Concluding remarks.....	114
4.3	Synthesis II: Preparation of BIT bulk samples by PLTC .....	114
4.3.1	Effect of hydrolysis temperature .....	114

4.3.1.1	TG/DTA .....	115
4.3.1.2	XRD analysis.....	117
4.3.1.3	Raman analysis.....	121
4.3.1.4	FTIR analysis.....	124
4.3.1.5	BET analysis.....	126
4.3.1.6	Particle morphology .....	126
4.3.1.7	TEM analysis.....	128
4.3.2	Effect of pH precursor .....	129
4.3.2.1	XRD analysis.....	129
4.3.2.2	Raman analysis.....	132
4.3.2.3	BET analysis.....	133
4.3.3	Effect of sintering temperature .....	134
4.3.3.1	Dilatometry analysis.....	134
4.3.3.2	Phase stability and grain orientation.....	135
4.3.3.3	Grain microstructures .....	137
4.3.3.4	Relative density- apparent porosity.....	139
4.3.3.5	Dielectric properties .....	140
4.3.3.6	Ferroelectric properties.....	142
4.3.4	Concluding remarks.....	145
4.3.5	Comparison of BIT properties by different methods.....	145
4.4	Synthesis III: Preparation of rare-earth substituted-BIT bulk samples ...	146
4.4.1	Effect of various molarities of La content .....	147
4.4.1.1	XRD analysis.....	147
4.4.1.2	Raman analysis.....	150
4.4.1.3	FTIR analysis.....	151
4.4.1.4	Particle morphology .....	153
4.4.1.5	Phase stability and grain orientation.....	154
4.4.1.6	Grain microstructures .....	155
4.4.1.7	XPS analysis.....	156
4.4.1.8	PL analysis.....	160
4.4.1.9	Dielectric properties .....	162
4.4.1.10	Ferroelectric properties.....	165
4.4.2	Concluding remarks.....	166
4.4.3	Effect of various rare-earth substitution systems.....	167

4.4.3.1	XRD analysis.....	167
4.4.3.2	Raman analysis.....	172
4.4.3.3	Particle morphology .....	173
4.4.3.4	Phase stability and grain orientation.....	175
4.4.3.5	Grain microstructures .....	177
4.4.3.6	PL analysis.....	179
4.4.3.7	Dielectric properties .....	181
4.4.3.8	Ferroelectric properties.....	185
4.4.4	Concluding remarks.....	190
CHAPTER 5	.....	191
5.1	Conclusions .....	191
5.2	Future Prospective .....	194
REFERENCES	.....	196
LIST OF PUBLICATION	.....	212
APPENDIX A	.....	215
APPENDIX B	.....	216
APPENDIX C	.....	217
APPENDIX D	.....	220
APPENDIX E	.....	223
APPENDIX F	.....	226

## LIST OF TABLE

		Pages
Table 2.1	Particle morphologies of BIT prepared by various processing methods	18
Table 2.2	Parameter studies and ferroelectric properties of BIT thin/thick films	27
Table 2.3	Electrical properties of substituted on A-site BIT ceramics using the conventional solid state reaction	30
Table 2.4	Electrical properties of various substitutions on A-site BIT thin films	32
Table 2.5	Electrical properties of ion substitution on B-site	38
Table 2.6	Merits and drawbacks of various processing methods	42
Table 2.7	Applications of functional materials	57
Table 3.1	General information of chemicals	64
Table 3.2	General information of analyzer used to measure the dielectric properties	83
Table 3.3	The details of tester unit	85
Table 4.1	Refinement of BIT powders with different Ti excess	90
Table 4.2	Refinement of BIT powders with different calcination temperature	102
Table 4.3	Observation on precursor solution at different hydrolysis temperature	115
Table 4.4	Possible crystal structures of BIT	120
Table 4.5	Refinement of BIT powders with different hydrolysis temperature	121
Table 4.6	Raman modes of BIT powders prepared by different methods	123
Table 4.7	The FTIR bands of BIT powders prepared by different methods	125
Table 4.8	Combustion time and maximum combustion temperature at different pH	129
Table 4.9	Refinement of BIT powders with different pH	131
Table 4.10	Properties of BIT powders and ceramics from different methods	146
Table 4.11	Refinement analysis of BLaT powders	149
Table 4.12	Ionic radius of Bi <sup>3+</sup> and other rare-earth elements	170
Table 4.13	Dielectric properties and Curie temperature	185
Table 5.1	Properties of BIT powders and ceramics from SGAC and PLTC	192
Table 5.2	Dielectric and ferroelectric properties of BIT, BLaT, BNdT and BSMT ceramics	194

## LIST OF FIGURE

		Pages
Figure 1.1	Schematic diagram for scope of research	8
Figure 2.1	Schematic representation of (a) charge stored on capacitor plates for a vacuum and (b) the increased charge storing capacity resulting from the polarization of a dielectric material	10
Figure 2.2	Variation of dielectric constant with frequency of an alternating electric field. Electronic, ionic and orientation polarization contributions to the dielectric constant are indicated	11
Figure 2.3	Venn diagram of subclasses of dielectric materials	12
Figure 2.4	Ferroelectric hysteresis loop	13
Figure 2.5	Corner sharing octahedral structures: (a) perovskite, (b) pyrochlore, (c) tungsten bronze and (d) bismuth layer	15
Figure 2.6	Schematic presentation of crystal structure of an Aurivillius layered BIT compound	17
Figure 2.7	BIT powders with spherical shape and less agglomeration produced by hydrothermal route	19
Figure 2.8	(a) hard agglomeration at pH 3 and (b) soft agglomeration at pH 7	20
Figure 2.9	BIT nanoplates synthesized by hydrothermal method assisted PEG addition	21
Figure 2.10	SEM micrographs of BIT powders calcined for 2 h at (a) 600, 700, 800 and 900°C	22
Figure 2.11	SEM of thermally etched surfaces of sintered BIT samples with and without magnetic alignment	23
Figure 2.12	Dielectric constant of BIT ceramics measured at different direction	24
Figure 2.13	Mechanism of vacancy formation in BIT at high temperatures	29
Figure 2.14	XRD patterns of the BLT thin films annealed at different temperatures ranging from 550 to 700°C for 30 min in oxygen	33
Figure 2.15	Hysteresis loops of BLT thin films annealed by different annealing conditions: (a) CTA (a) and (b) RTA	34
Figure 2.16	The modes of combustion synthesis: (a) SHS and (b) VCS	50
Figure 2.17	Flow diagram for preparation of oxide materials by solution combustion synthesis	52
Figure 2.18	Ion distribution of citric acid at different pH	56
Figure 2.19	Memory classification	58
Figure 2.20	DRAM operation with ferroelectric capacitor	60
Figure 3.1	Parameter studied for optimization in SGAC and PLTC methods	65

Figure 3.2	Powder preparation of BIT via SGAC	67
Figure 3.3	Powder preparation of BIT via PLTC	69
Figure 3.4	Powder preparation of rare-earth substitution in BIT via PLTC	70
Figure 3.5	Ceramic fabrication of BIT and rare-earth substituted-BIT samples	72
Figure 3.6	A set of Sawyer-Tower circuit for ferroelectric hysteresis loop measurement. Inset shows the hysteresis loop that was displayed at oscillator	85
Figure 4.1	TG-DTA curves of as-dried powder prepared by SGAC	87
Figure 4.2	XRD patterns of BIT powders with: (a) 10 wt% Bi excess and different Ti excess: (b) 0 wt%, (c) 2 wt%, (d) 5 wt%, (e) 10 wt%, (f) 15 wt%, calcined at 750°C for 3 hours	89
Figure 4.3	Raman spectra of BIT powders prepared with different Ti excess: (a) 0 wt%, (b) 2 wt%, (c) 5 wt%, (d) 10 wt% and (e) 15 wt%	92
Figure 4.4	FTIR spectra of BIT powders with Ti excess: (a) 0 wt%, (b) 2 wt%, (c) 5 wt%, (d) 10 wt% and (e) 15 wt%	95
Figure 4.5	FESEM images of BIT powders prepared with: (a) 0 wt%, (b) 2 wt%, (c) 5 wt%, (d) 10 wt% and (e) 15 wt% Ti excess	97
Figure 4.6	XRD patterns of BIT powders calcined at different temperatures for 3 hours: (a) as-combusted, (b) 600°C, (c) 650°C, (d) 700°C, (e) 750°C and (f) 800°C	98
Figure 4.7	Evolution of XRD patterns with calcination temperature associated with the peaks (a): (020)/(200) and (b): (317)/(137)	101
Figure 4.8	FESEM images of BIT powders calcined at different temperatures: (a) as-combusted at 2.5 kX, (b) as-combusted at 10 kX, inset image taken at 25 kX, (c) 600°C, inset image taken at 25 kX, (d) 700°C and (e) 800°C	103
Figure 4.9	TEM images of BIT powders calcined at (a) 700°C, (b) 750°C, (c) 800°C and (d) SAD of sample calcined at 750°C	105
Figure 4.10	XRD patterns of BIT ceramics sintered at different temperatures for 3 hours: (a) 900°C, (c) 1000°C and (d) 1100°C	106
Figure 4.11	(117) had shifted to low $2\theta$ angle with the increase of sintering temperature: (a) 900°C, (c) 1000°C and (d) 1100°C	107
Figure 4.12	Surface grain microstructures of BIT ceramics sintered at different temperatures for 3 hours: (a) 900°C, (b) 1000°C, (c) 1100°C, (d) fracture surface of sample sintered at 1100°C at 2 kX and (e) fracture surface of sample sintered at 1100°C at 10 kX	108
Figure 4.13	Relative density and apparent porosity of BIT ceramics	110
Figure 4.14	Dielectric constant, $\epsilon_r$ of BIT ceramics with different sintering temperatures: (a) 900°C, (b) 1000°C and (c) 1100°C prepared by SGAC. Inset shows those at 1 MHz	111

Figure 4.15	Dielectric loss, $\tan \delta$ of BIT ceramics with different sintering temperatures: (a) 900°C, (b) 1000°C and (c) 1100°C prepared by SGAC. Inset shows those at 1 MHz	112
Figure 4.16	Ferroelectric hysteresis loops of BIT ceramic prepared by SGAC	113
Figure 4.17	TG of as-dried powders with different hydrolysis temperature: (a) 40°C, (b) 50°C and (c) 60°C	116
Figure 4.18	DTA of as-dried powders with different hydrolysis temperature: (a) 40°C, (b) 50°C and (c) 60°C	117
Figure 4.19	XRD patterns of BIT powders at different hydrolysis temperatures: (a) 40°C, (b) 50°C and (c) 60°C	118
Figure 4.20	XRD patterns of the powders prepared at 60°C with different conditions: (a) without calcination and (b) calcination at 500°C	119
Figure 4.21	Raman spectra of BIT powders synthesized at different hydrolysis temperatures: (a) 40°C, (b) 50°C and (c) 60°C	122
Figure 4.22	FTIR spectra of BIT powders prepared at different hydrolysis temperatures: (a) 40°C, (b) 50°C and (c) 60°C	124
Figure 4.23	FESEM of BIT powders prepared at different hydrolysis temperatures at low magnification of 10 kX: (a) 40°C, (b) 50°C and (c) 60°C	127
Figure 4.24	FESEM of BIT powders prepared at different hydrolysis temperatures at high magnification of 50 kX: (a) 40°C, (b) 50°C and (c) 60°C	127
Figure 4.25	HRTEM analysis on BIT powder prepared at 60°C: (a) TEM image, (b) interplanar spacing and (c) SAD image	128
Figure 4.26	XRD patterns of BIT powders with different pH: (a) uncontrolled, (b) pH 1, (c) pH 3, (d) pH 5, (e) pH 7 and (f) pH 9	130
Figure 4.27	Raman spectra of BIT powders with different pH	133
Figure 4.28	BET specific surface area of BIT powders with different pH	134
Figure 4.29	Dilatometry curve showing the shrinkage of sample dimension with different temperatures	135
Figure 4.30	XRD patterns of BIT ceramics sintered at different temperatures for 3 hour: (a) 800°C, (b) 900°C, (c) 1000°C and (d) 1100°C	136
Figure 4.31	Several peaks correspond to <i>c</i> -axis and (117)-axis orientation for various sintering temperatures: (a) 800°C, (b) 900°C, (c) 1000°C and (d) 1100°C	137
Figure 4.32	Surface microstructure of BIT ceramics sintered at different temperatures: (a) 800°C, (b) 900°C, (c) 1000°C, (d) 1100°C	138
Figure 4.33	Relative density and apparent porosity of BIT ceramics	139
Figure 4.34	Dielectric constant, $\epsilon_r$ of BIT ceramics with different sintering temperature (a) 800, (b) 900, (c) 1000 and (d) 1100°C measured at different frequency. Inset shows those at 1 MHz	141

Figure 4.35	Dielectric loss, $\tan \delta$ of BIT ceramics with different sintering temperature (a) 800, (b) 900, (c) 1000 and (d) 1100°C measured at different frequency. Inset shows those at 1 MHz	142
Figure 4.36	Ferroelectric hysteresis loops of BIT ceramics sintered at 900°C as a function of applied voltage	143
Figure 4.37	Ferroelectric hysteresis loops of BIT ceramics with different sintering temperature	144
Figure 4.38	XRD patterns of: (a) BIT, (b) BLaT25, (c) BLaT50, (d) BLaT75 and (e) BLaT100 powders	148
Figure 4.39	Peak splitting of (020)/(200) and (317)/(137) reflections with different samples: (a) BIT, (b) BLaT25, (c) BLaT50, (d) BLaT75 and (e) BLaT100 powders	148
Figure 4.40	Raman spectra of: (a) BIT, (b) BLaT25 and (c) BLaT75 powders	151
Figure 4.41	FTIR spectra of: (a) BIT, (b) BLaT25 and (c) BLaT75 powders	152
Figure 4.42	Particle morphology of: (a) BLaT25, (b) BLaT50, (c) BLaT75 and (d) BLaT100 powders. Inset shows TEM image of BLaT25 (red circle indicates the presence of single particle in nanoscale)	153
Figure 4.43	XRD patterns of: (a) BIT, (b) BLaT25, (c) BLaT50, (d) BLaT75 and (e) BLaT100 ceramics	154
Figure 4.44	(117) had shifted to high $2\theta$ angle with increasing La content: (a) BIT, (b) BLaT25, (c) BLaT50, (d) BLaT75 and (e) BLaT100	155
Figure 4.45	SEM images of La substituted-BIT ceramics: (a) BLaT25, (b) BLaT50, (c) BLaT75 and (d) BLaT100	156
Figure 4.46	XPS spectra of (a) BIT and (b) BLaT100 ceramics	157
Figure 4.47	Core level photoemission of BLaT100 compound: (a) Bi 4f, (b) Bi 4d and Ti 2p, (c) La 3d and (d) O 1s	159
Figure 4.48	Deconvolution of the PL spectra of (a) BIT, (b) BLaT25, (c) BLaT100 ceramics and (d) PL spectra of BIT and BLaT ceramics	161
Figure 4.49	Dielectric constant, $\epsilon_r$ of: (a) BIT, (b) BLaT25, (c) BLaT50, (d) BLaT75 and (e) BLaT100 measured at different frequencies. Inset showing the dielectric constant at 1 MHz	163
Figure 4.50	Dielectric loss, $\tan \delta$ of BIT and BLaT ceramics as a function of frequency	164
Figure 4.51	Ferroelectric hysteresis loops of BLaT ceramics	165
Figure 4.52	Remanent polarization, $P_r$ and coercive field, $E_c$ of BLaT ceramics	166
Figure 4.53	XRD patterns of BNdT and BSmT powders with different molarities: (a) 0.25, (b) 0.50, (c) 0.75 and (d) 1.0	168
Figure 4.54	XPS spectra of Sm 3d core level for BSmT100 ceramic	169

Figure 4.55	Variation of lattice parameters, unit cell volume and crystallite sizes of Nd (a and b) and Sm (c and d) substitution system	171
Figure 4.56	Raman spectra of: (a) BLaT, (b) BNdT and (c) BSmT with different molarities of 0.25 and 0.75	172
Figure 4.57	Raman shift for different modes of rare-earth substitution systems with different molarities: (a) 0.25 and (b) 0.75	173
Figure 4.58	FESEM images of BNdT powders with different Nd content: (a) 0.25, (b) 0.50, (c) 0.75 and (d) 1.0	174
Figure 4.59	FESEM images of BSmT powders with different Sm content: (a) 0.25, (b) 0.50, (c) 0.75 and (d) 1.0	174
Figure 4.60	XRD patterns of BNdT and BSmT ceramics with different molarities: (a) 0.25, (b) 0.50, (c) 0.75 and (d) 1.0, and subsequently, sintered at 1000°C for 3 hours	176
Figure 4.61	Grain morphologies of BNdT ceramics with different Nd content: (a) 0.25, (b) 0.50, (c) 0.75 and (d) 1.0	178
Figure 4.62	Grain morphologies of BSmT ceramics with different Sm content: (a) 0.25, (b) 0.50, (c) 0.75 and (d) 1.0	178
Figure 4.63	Deconvolution of line shape for (a) BNdT25, (b) BNdT100, (c) BSmT25, (d) BSmT100, PL spectra of (e) BNdT system	180
Figure 4.64	Dielectric properties of rare-earth substitution ceramics at 1 MHz: (a) dielectric constant, $\epsilon_r$ and (b) dielectric loss, $\tan \delta$	182
Figure 4.65	Temperature dependence of dielectric properties for rare-earth substitution ceramics with 0.75: (a) dielectric constant, $\epsilon_r$ and (b) dielectric loss, $\tan \delta$	183
Figure 4.66	Lattice <i>a</i> - and <i>b</i> - parameters almost close with increasing rare-earth content: (a) Nd and (b) Sm	184
Figure 4.67	Ferroelectric hysteresis loops of BNdT and BSmT ceramics with different molarities content: (a) 0.25, (b) 0.50 and (c) 0.75 and (d) 1.0	186
Figure 4.68	(a) Remanent polarization, $P_r$ and (b) coercive field, $E_c$ of BIT and various rare-earth substitutions	187
Figure 4.69	Electronic configuration of rare-earth elements: (a) La, (b) Nd and (c) Sm	188
Figure 4.70	Frequency dependence of ferroelectric hysteresis loops for BLaT75 ceramic	190

## LIST OF ABBREVIATIONS

Bi	Bismuth
Ti	Titanium
O	Oxygen
La	Lanthanum
Nd	Neodymium
Sm	Samarium
C	Carbon
H	Hydrogen
BIT	Bismuth titanate
BLaT	La substituted-BIT
BNdT	Nd substituted-BIT
BSmT	Sm substituted-BIT
SGAC	Sol-gel auto-combustion
PLTC	Precipitation assisted low-temperature combustion
FESEM	Field emission scanning electron microscopy
XRD	X-ray diffraction
TEM	Transmission electron microscopy
HRTEM	High resolution transmission electron microscopy
SAD	Selected area diffraction
FTIR	Fourier transform infrared spectroscopy
TG	Thermogravimetry
DTA	Differential thermal analysis
XPS	X-ray photoelectron spectroscopy
PL	Photoluminescence
PDF	Powder diffraction file
FWHM	Full-width-half-maximum
FRAM	Ferroelectric random access memory
DRAM	Dynamic random access memory
ASTM	American Society for Testing and Materials

## LIST OF SYMBOLS

$\theta$	Theta
$^{\circ}\text{C}$	Degree Celsius
%	Percent sign
$\epsilon_r$	Dielectric constant
$\tan \delta$	Dielectric loss
P	Polarization
E	Electric field
$P_r$	Remanent polarization
$P_s$	Spontaneous polarization
$E_c$	Coercive field
$T_c$	Curie temperature
$R_{wp}$	Weighted profile <i>R</i> -factor
$R_{exp}$	Expected <i>R</i> -factor
GOF	Goodness-of-fit
<i>S</i>	Goodness-of-fit indicator
$\mu\text{m}$	Micrometre
nm	Nanometer
$\mu\text{C}$	Microcoulomb
mg	Milligram
cm	Centimetre
kV	Kilovolts
Hz	Hertz
kHz	Kilohertz
MHz	Megahertz
<i>r</i>	Ionic radius
eV	Electronvolt
Å	Angstrom
MPa	Megapascal

**KESAN TUKAR GANTI NADIR BUMI TERHADAP SIFAT-SIFAT  
BISMUTH TITANAT YANG DIHASILKAN MELALUI TEKNIK  
PEMBAKARAN BERSUHU RENDAH**

**ABSTRAK**

Dalam kerja penyelidikan ini, penghasilan bismuth titanat ( $\text{Bi}_4\text{Ti}_3\text{O}_{12}$  atau BIT) pada suhu rendah melalui kaedah pembakaran telah dikaji bagi mengurangkan pembebasan Bi yang merendahkan sifat-sifat dielektrik dan ferroelektrik. Bagi mengatasi masalah tersebut, dalam fasa pertama, dua kaedah pembakaran; auto-pembakaran sol-gel (SGAC) dan pemendakan dibantu pembakaran suhu-rendah (PLTC) telah dikaji dari sudut pembentukan fasa, struktur, morfologi partikel dan ira, sifat-sifat dielektrik dan ferroelektrik. Penggunaan SGAC telah menghasilkan fasa tunggal BIT dengan darjah penghabluran yang tinggi pada  $750^\circ\text{C}$ , saiz partikel iaitu 120 nm, berbentuk bulat dengan ketumpatan relatif paling tinggi sebanyak 84% pada  $1100^\circ\text{C}$ . Pemalar dielektrik ( $\epsilon_r$ ), kehilangan dielektrik ( $\tan \delta$ ), pengutuban bakian ( $P_r$ ) dan medan koersif ( $E_c$ ) bagi BIT melalui SGAC adalah 119, 0.008,  $6.3 \mu\text{C}/\text{cm}^2$  and 20 kV/cm, masing-masing. Bagi PLTC, fasa tunggal BIT dengan penghabluran yang tinggi terbentuk sekitar  $290^\circ\text{C}$  tanpa pengkalsinan, dengan saiz partikel iaitu 50 nm yang berbentuk kepingan. Ketumpatan paling tinggi sebanyak 86% telah dicapai pada  $1000^\circ\text{C}$ . Nilai-nilai  $\epsilon_r$ ,  $\tan \delta$ ,  $P_r$  and  $E_c$  bagi BIT melalui PLTC adalah 113, 0.007,  $6.8 \mu\text{C}/\text{cm}^2$  and 26 kV/cm, masing-masing. Untuk fasa kedua, BIT dengan tukar ganti nadir bumi telah dikaji dan dijumpai bahawa La dan Nd menunjukkan pencirian yang sama, yang mana kedua-duanya telah menghasilkan fasa tunggal tanpa bersandarkan kandungan La dan Nd. Kehadiran fasa pirokloro telah dikesan dalam sampel BSmT apabila kandungan Sm melebihi 0.5. BIT dengan tukar ganti La

(BLaT100) telah menunjukkan  $\epsilon_r$  yang tinggi (212) dan  $\tan \delta$  yang rendah (0.005). Ini disebabkan keseragaman saiz ira (1.6  $\mu\text{m}$  panjang and 0.3  $\mu\text{m}$  lebar) dengan penambahbaikan ketumpatan relatif (91%) sampel. Walau bagaimanapun, untuk sifat ferroelektrik,  $P_r$  yang maksimum (9.6  $\mu\text{C}/\text{cm}^2$ ) dengan  $E_c$  yang rendah (18 kV/cm) telah diperhatikan pada sampel-sampel BLaT75 dan BLaT100, masing-masing. Sampel paling optimum untuk BIT dengan tukar ganti Nd adalah BNdT100 dengan nilai-nilai  $\epsilon_r$  dan  $\tan \delta$  adalah 231 dan 0.005, masing-masing. Purata saiz ira sebanyak 1.3  $\mu\text{m}$  panjang dan 0.3  $\mu\text{m}$  lebar dengan penambahbaikan ketumpatan relatif sekitar 90% telah dicapai pada sampel BNdT100. Bagi sifat ferroelektrik,  $P_r$  yang maksimum (9.2  $\mu\text{C}/\text{cm}^2$ ) dengan  $E_c$  yang rendah (34 kV/cm) telah diperhatikan pada sampel-sampel BNdT75 and BNdT100, masing-masing. Bagi sistem BSmT, penambahbaikan pemalar dielektrik telah diperhatikan daripada sampel BSmT100 dengan nilai  $\epsilon_r$  dan  $\tan \delta$  adalah 139 and 0.004, masing-masing. Penambahbaikan keputusan dielektrik telah disebabkan keseragaman saiz ira (1.9  $\mu\text{m}$  panjang dan 0.4  $\mu\text{m}$  lebar). Namun begitu, prestasi ferroelektrik yang menurun bagi BSmT100 adalah disebabkan  $P_r$  yang rendah (4.4  $\mu\text{C}/\text{cm}^2$ ) dan  $E_c$  yang tinggi (64.3 kV/cm).

**THE EFFECT OF RARE-EARTH SUBSTITUTION ON THE PROPERTIES  
OF BISMUTH TITANATE PREPARED BY LOW TEMPERATURE  
COMBUSTION TECHNIQUE**

**ABSTRACT**

In this research work, the production of bismuth titanate ( $\text{Bi}_4\text{Ti}_3\text{O}_{12}$  or BIT) at low temperature using combustion method was investigated to minimize the volatilization of Bi that deteriorates the dielectric and ferroelectric properties. In order to embark upon this problem, in the first phase, two combustion methods; sol-gel auto-combustion (SGAC) and precipitation assisted low-temperature combustion (PLTC) were investigated in terms of phase formation, structural, powder and grain morphology, dielectric and ferroelectric properties. The use of SGAC had resulted in single phase BIT with high degree of crystallinity at  $750^\circ\text{C}$ , particle size of 120 nm, spherical in shape with the highest relative density of about 84% at  $1100^\circ\text{C}$ . The dielectric constant ( $\epsilon_r$ ), dielectric loss ( $\tan \delta$ ), remanent polarization ( $P_r$ ) and coercive field ( $E_c$ ) of BIT by SGAC were 119, 0.008,  $6.3 \mu\text{C}/\text{cm}^2$  and 20 kV/cm, respectively. For PLTC, the single phase BIT with high crystallinity was formed at around  $290^\circ\text{C}$  without calcination, with particle size of 50 nm which is platey in shape. The highest relative density of 86% was achieved at  $1000^\circ\text{C}$ . The values of  $\epsilon_r$ ,  $\tan \delta$ ,  $P_r$  and  $E_c$  of BIT by PLTC were 113, 0.007,  $6.8 \mu\text{C}/\text{cm}^2$  and 26 kV/cm, respectively. For the second phase, rare-earth substituted-BIT was investigated and it was found that La and Nd exhibited similar characteristic, whereby both resulted in single phase regardless of La and Nd content. The presence of pyrochlore phase was detected in BSmT samples when the content Sm above 0.5. La substituted-BIT (BLaT100) exhibited high  $\epsilon_r$  (212) and low  $\tan \delta$  (0.005). This is

as a result of uniform grain size (1.6  $\mu\text{m}$  in length and 0.3  $\mu\text{m}$  in width) with the improved relative density (91%) of the sample. However, for ferroelectric properties, the maximum  $P_r$  (9.6  $\mu\text{C}/\text{cm}^2$ ) with low  $E_c$  (18 kV/cm) were observed at BLaT75 and BLaT100 samples, respectively. The best optimum sample for Nd substituted-BIT was BNdT100 with  $\epsilon_r$  and  $\tan \delta$  values of 231 and 0.005, respectively. The average grain size was 1.3  $\mu\text{m}$  in length and 0.3  $\mu\text{m}$  in width with improved relative density of 90% were achieved in BNdT100 sample. For ferroelectric properties, the maximum  $P_r$  (9.2  $\mu\text{C}/\text{cm}^2$ ) with low  $E_c$  (34 kV/cm) were identified from BNdT75 and BNdT100 samples, respectively. In BSmT system, the improved dielectric properties were obtained from BSmT100 sample with  $\epsilon_r$  and  $\tan \delta$  were 139 and 0.004, respectively. The improved dielectric results were attributed to the uniform grain size (1.9  $\mu\text{m}$  in length and 0.4  $\mu\text{m}$  in width). Nevertheless, the low ferroelectric performance in BSmT100 is due to low  $P_r$  (4.4  $\mu\text{C}/\text{cm}^2$ ) and high  $E_c$  (64.3 kV/cm).

# CHAPTER 1

## INTRODUCTION

### 1.1 Research background

Lead-free ceramics have been widely used as ferroelectric materials due to environmental friendly for their less toxicity. Many researchers have greatly focused on the lead-free ceramics to replace the lead-based ceramics such as lead titanate ( $\text{PbTiO}_3$  or PT) and lead zirconate titanate ( $\text{Pb}(\text{Zr,Ti})\text{O}_3$  or PZT). Layer-structured perovskite-like barium titanate ( $\text{BaTiO}_3$  or BT), strontium titanate ( $\text{SrTiO}_3$  or ST), barium strontium titanate ( $(\text{Ba,Sr})\text{TiO}_3$ ) or BST), strontium bismuth tantalate ( $\text{SrBi}_2\text{Ta}_2\text{O}_9$  or SBT) and bismuth titanate ( $\text{Bi}_4\text{Ti}_3\text{O}_{12}$  or BIT), those are a group of lead-free ferroelectrics. Among these ceramics, BIT has received special attention due to its potential for the development of memory technology such as dynamic random access memory (DRAM) and ferroelectric random access memories (FRAM) (Park et al., 1999). Moreover, the interesting electro-optic properties and the high Curie temperature ( $675^\circ\text{C}$ ) of this material allow its use in high temperature piezoelectric components and optical displays (Jardiel et al., 2008; Oliveira et al., 2009).

In general, BIT is a member of Aurivillius compound which can be prepared in different forms such as thick and thin films, ceramics and single crystal. Nowadays, ferroelectric thin films and ceramics have attracted much attention for various studies which are used for numerous potential applications (Besland et al., 2006; Yang et al., 2008). Nevertheless, the preparation methods thin films and ceramics are rather

obviously different. Normally, the deposition of thin films is more complex to obtain a good layer on substrate. In order to tackle this problem, high precision deposition technique is essential in order to control the desired thickness and surface layer of ferroelectric compounds. To date, physical vapor deposition (PVD), chemical vapor deposition (CVD), metal-organic chemical vapor deposition (MOCVD) and RF sputtering have been frequently used to obtain a better ferroelectric thin films condition. However, a major concern on expensive equipment and experience user limit this technique in many studies. In order to develop the ferroelectric materials, the preparation of bulk ceramics has been studied.

BIT is known as a ferroelectric material to have a high Curie temperature ( $T_c = 675^\circ\text{C}$ ), high dielectric constant ( $\epsilon_r = 100 - 200$ ), low dielectric loss ( $\tan \delta = 0.005 - 0.05$ ), high remanent polarization ( $P_r = 5 - 7 \mu\text{C}/\text{cm}^2$ ) and low coercive field ( $E_c = 20 - 50 \text{ kV}/\text{cm}$ ) (Zhi-hui et al., 2010; Herrera Robles et al., 2012). In addition, the spontaneous polarization ( $P_s$ ) of BIT single crystal are 50 and  $4 \mu\text{C}/\text{cm}^2$  along the a-axis and c-axis, respectively (Kao et al., 2008a). However, several shortcomings of BIT limit its capability for more advanced applications. It was reported by Xiang et al. (2005) that Bi ions, located at A-site in  $\text{ABO}_3$  BIT structure, is known to be unstable due to easily volatile during sintering at temperature above  $1000^\circ\text{C}$ . Park et al. (1999) stated that the oxygen near the Bi ions is likely to be less stable due to the volatility of the Bi ions. Thus, defects, such as bismuth vacancies ( $\text{VBi}'''$ ) and oxygen vacancies ( $\text{Vo}''$ ), could exist in the perovskite layers and act as a space charge. The presence of space charge implies that BIT has critical drawbacks on its ferroelectric properties such as high leakage current and domain pinning which leads to small remanent polarization and low fatigue

endurance. Therefore, optimization or solution to resolve aforementioned drawbacks needs comprehensive investigation. In general, the improved properties of BIT can be achieved by ion substitution and improving the processing route. With this regard, the present work is more focussed on the improvement of ferroelectric properties using both corresponding factors.

Ion substitution is a feasible method to improve the stability structure of BIT which also resulted in better ferroelectric properties. In principle, the substitution in BIT can be performed on Bi ions (or A-site), Ti ions (or B-site) or both sites. Based on reports by Lv et al. (2005) and Yao et al. (2004), the substitution on any sites in BIT showed the different effect on the ferroelectric properties. Nevertheless, Wang et al. (2009) reported that the substitution of Bi ions at A-site is more effective than Ti ions at B-site in enhancing the ferroelectric properties. This is because that the B-site cations are similar in size and do not plays a major structural role in the polarization process of BIT. In comparison to earlier report by Li et al. (2005), the orbital hybridization is a mainly root cause for the enhancement of remanent polarization instead of substitution ionic radius size.

Based on different viewpoints, a study on the improvement of ferroelectric by ion substitution is very interesting. For many cases, the ion substitution on A-site is more suitable by any elements that possess a similar ion valences. On this basis, the rare-earth elements such as La, Nd, Sm, Pr, Eu and Dy ions are more preferred dopant for Bi ions in BIT. In principle, the role of substitution is to displace the volatile Bi ions with rare-earth element which in turn to suppress the Bi vacancies accompanied by oxygen vacancies (Simões et al., 2004a). In other words, the space

charge effect can be minimized and subsequently, resulted in large remanent polarization and good fatigue endurance after switching cycles.

Improvement in processing route can also become another solution to improve the stability of BIT structure and subsequently, the ferroelectric properties. As stated earlier, the Bi ions are volatile at high temperature. In simple method, the BIT powders have been prepared using the conventional solid state reaction (Kumar & Buddhudu, 2010). Nevertheless, this conventional method produces non-stoichiometric composition due to the undesirable loss of Bi content through volatilization at elevated temperature thus, reducing the ferroelectric properties of BIT. In addition, this method also causes crystallites coarsening and particle aggregation due to calcination at high temperature. Hence, the volatility issue can probably be minimized by using wet chemical synthesis such as hydrothermal method, sol-gel method, precipitation method and mechanosynthesis.

The advantages of the wet chemical synthesis over the conventional solid state reaction are the controlled morphology, narrow particle size distribution, high purity, high crystallinity and possible reduction in calcination and sintering temperatures. Besides, the possibility to minimize the volatility issue can also be carried out by simplifying the processing route such as eliminate calcination step which then produces nanosized powder with improved sinterability. At this moment, the popular methods such as hydrothermal method and mechanosynthesis have been widely used to produce BIT ceramics. Nevertheless, the studies on rare-earth substituted-BIT ceramics are very limited from both methods. In addition to that, the hydrothermally powder is typically synthesized at high pressure using a high quality Teflon-lined

stainless steel autoclave in longer reaction time (Pookmanee et al., 2004a). Besides, the mechanically activated powders prepared from mechanosynthesis is tough to form a single crystalline structure of Bi-layered due to improper set up on several milling parameters such as impact energy, impact frequency, milling intensity and energy dose (Zdujić et al., 2009).

Self-sustaining combustion synthesis has emerged as an essential technique for the synthesis and processing of structural and functional ceramics, catalysts, composite, alloys, intermetallics and nanomaterials. According to Aruna & Mukasyan (2008), this method is convenient in process, simple in experimental device and saving in time and energy consumption in comparison to the conventional solid state reaction and several wet chemical routes. Moreover, it is a straightforward preparation process to produce homogeneous, very fine, crystalline and unagglomerated multi-component oxide powders without intermediate decomposition steps (da Silva et al., 2011). Patil et al. (2002) reported that the important key of combustion synthesis is highly dependent on the interaction of three important elements such as oxidizer, fuel agent and temperature. A good interaction between these three elements leads to the production of ceramic powders at lower temperature and shorter reaction time.

On this basis, an attempt has been made to synthesis BIT powders via combustion technique. So far, little work has been done to study BIT powder produced by this technique. To the best of our knowledge, Macedo et al. (2004a) reported that the BIT powders was produced using two different fuel agents i.e. urea and polysaccharide in a short reaction time. However, the quality of the BIT powders

was strongly dependent on sintering conditions between 800 and 1000°C for 30 minutes. In addition, the presence of intermediate phases such as  $\text{Bi}_{12}\text{TiO}_{20}$  and  $\text{Bi}_2\text{Ti}_4\text{O}_{11}$  were also identified after sintering step. From this study, it implies that the formation of a single crystalline structure of Bi-layered at temperature as low as possible is another challenge which has to be systematically solved using different parameter studies of combustion route.

With this background, this research was embarked to synthesize BIT and rare-earth substituted-BIT powders by the combustion technique. In order to identify more reliable information on combustion synthesis, the BIT powders were synthesized using two different combustion methods i.e. the sol-gel auto-combustion (SGAC) and precipitation assisted low-temperature combustion (PLTC). In order to overcome the volatility issue in BIT, the incorporation of La, Nd and Sm ion elements in the BIT structure was studied. Finally, the functional properties such as dielectric and ferroelectric properties were also investigated.

## **1.2 Problem statement**

As described earlier, BIT has a great performance as dielectric and ferroelectric materials. However, there are several problems which limit its applications. These can be addressed in the following points:

- i) Processing route: high calcination is typically subjected to the powders, leading to hard aggregates with low sinterability,
- ii) Inherent defect: Volatility issue during sintering process, leading to oxygen and bismuth vacancies.

### **1.3 Research objectives**

Several objectives are listed as follows:

- i) To synthesize BIT powders at low temperature ( $<500^{\circ}\text{C}$ ) using the combustion technique and subsequently, characterize their properties
- ii) Investigate the effect of La, Nd and Sm addition on the properties of BIT
- iii) Study the improvement of dielectric and ferroelectric properties as a result of substitution effect

### **1.4 Scope of research**

In order to get more insight in terms of material science and engineering, this research is systematically designed to cover the synthesis (processing method), structure (composition), properties and performance as depicted in Figure 1.1. In general, this work is more focussed on synthesis and characterization of BIT and rare-earth substituted-BIT ceramics. Initially, the BIT powders were synthesized using the SGAC method using two different parameter studies; i.e. effect of Ti excess and effect of calcination temperature. The obtained powders were finally sintered at different temperatures, which is typically higher than the calcination temperature of BIT powder. In addition, another batch of BIT powders were synthesized using PLTC method with different parameter studies; i.e. effect of pH and effect of hydrolysis temperature.

The optimized method was then used to investigate the effect of rare-earth substituted-BIT. Substitution on A-site in BIT (also referred as substitution for Bi ions) was initially carried out using La content with different molarities; 0.25, 0.50,

0.75 and 1.0. Selection on La was firstly reported due to its ionic radius ( $r = 0.116 \text{ nm}$ ) is very close to Bi ( $r = 0.117 \text{ nm}$ ) which is compatible for ionic substitution. With regards to smaller ionic radius, another two different rare-earth elements; Nd ( $r = 0.111 \text{ nm}$ ) and Sm ( $r = 0.108 \text{ nm}$ ) were investigated. The performance of dielectric and ferroelectric properties was compared among rare-earth substituted-BIT ceramics.

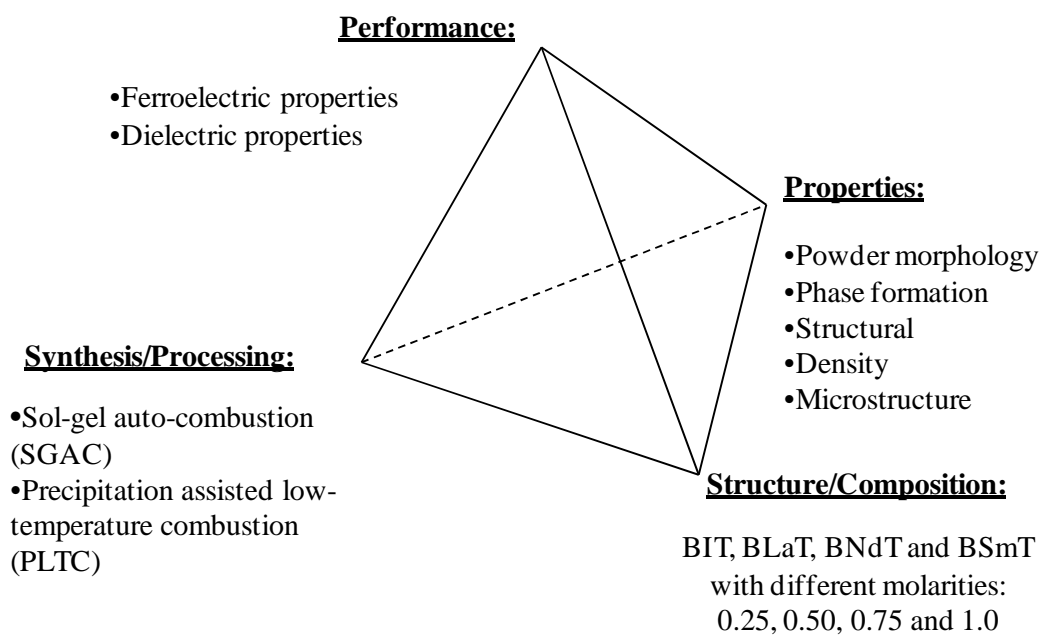


Figure 1.1: Schematic diagram for scope of research

## CHAPTER 2

### LITERATURE REVIEW

#### 2.1 Introduction

Electroceramics are ceramic materials that are specially formulated for several functional materials such as dielectric, conductive, magnetic or optical circuit applications. The unique properties of electroceramics have made increasingly important materials in many key technologies including communications, energy conversion, storage, electronics and automation. In general, electroceramics can be broadly divided into two major groups i.e. dielectric and conductive ceramics (Setter, 2001). Dielectric ceramics includes linear and non-linear dielectrics while conductive ceramics are superconductors, conductors and semiconductors.

#### 2.2 General concept of functional materials

Dielectrics are generally known as a class of material with high polarizability, whereby they can perform insulating functions by an applied electric field. In general, the dielectrics can be used for various functional materials with the presence of an electric field. In principle, the distance of positive and negative electric charge is associated to electric dipole moment. The simplest practical application can be used as a capacitor, whereby the ability to store charges (also corresponds to capacitance,  $C$ ) is related to the process of dipole alignment or polarization under the electrical field. The magnitude of storage capability is called as dielectric constant (relative permittivity,  $\epsilon_r$ ). Figure 2.1 shows a simplified model of polarization within a dielectric material, whereby the entire solid within the plates becomes polarized when an electric field is applied. This phenomenon is also called as dielectric

polarization, whereby the positive charges are displaced toward the field and negative charges shift in the opposite direction.

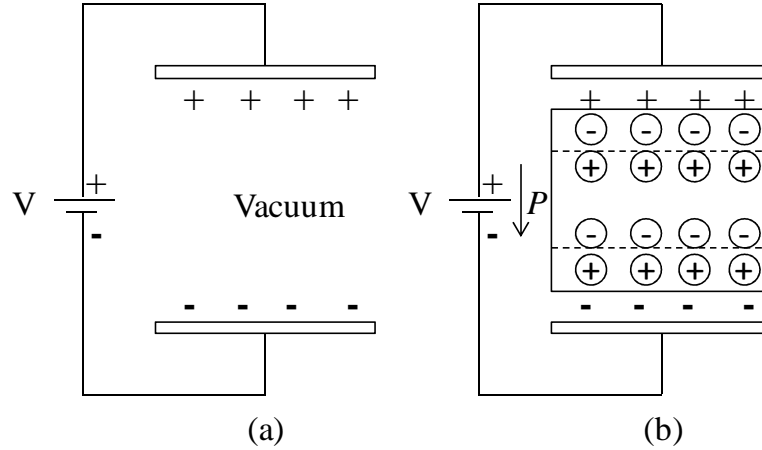


Figure 2.1: Schematic representation of (a) charge stored on capacitor plates for a vacuum and (b) the increased charge storing capacity resulting from the polarization of a dielectric material (Callister, 2007)

Generally, there are five sources of polarization which can contribute to the dielectric response, namely electronic polarization, ionic polarization, orientation polarization, space charge polarization and domain wall polarization (Böttger, 2005). Electronic polarization may be formed in all dielectric materials that result from a displacement of electron cloud by an electric field (Callister, 2007). Ionic polarization is a phenomenon in ionic materials that are attributed to the relative displacement of electrically charged with the presence of electric field. Orientation polarization is a response of permanent electric dipoles to an applied electric field that eventually resulted in one direction. Space charge polarization can be ascribed to the inhomogeneity of charge carried densities in dielectric materials. Domain wall polarization is an essential source of polarization in ferroelectric materials that favored oriented domains in response to an applied field (Böttger, 2005). The influence of dielectric constant on the frequency is illustrated in Figure 2.2.

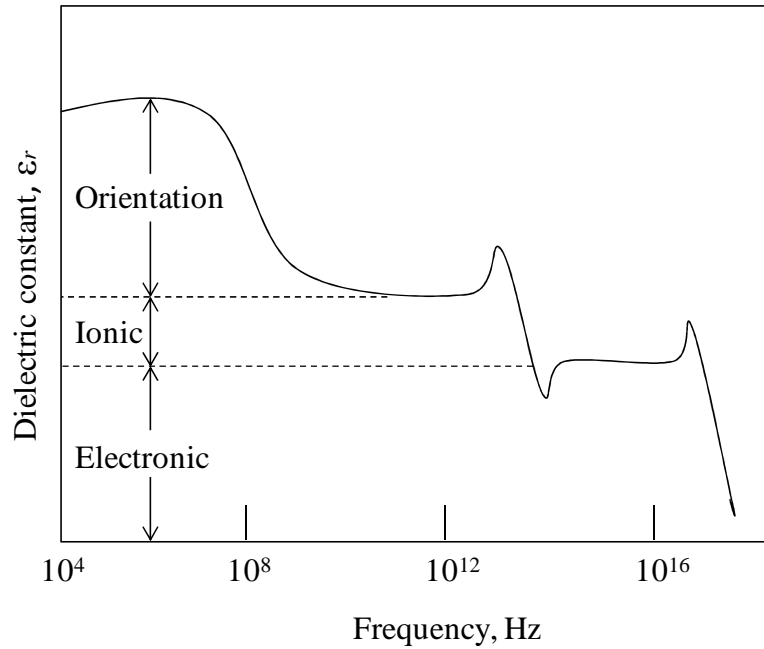


Figure 2.2: Variation of dielectric constant with frequency of an alternating electric field. Electronic, ionic and orientation polarization contributions to the dielectric constant are indicated (Callister, 2007)

Other functional groups of dielectric materials are piezoelectric materials, whereby the polarization is contributed from mechanical stress instead of electric field. The magnitude of the polarization rely on the magnitude of stress, while the sign of the charge produced depend on the type of stress, i.e. tensile or compressive (Jardiel et al., 2008). Some piezoelectric materials are characterized as pyroelectric materials. These materials exhibit electric dipole moment in the absence of an electric field. The polarization associated with a spontaneously formed dipole moment is called spontaneous polarization. The change of spontaneous polarization with temperature describes the pyroelectric effect (Damjanovic, 1998). Some pyroelectric materials have an additional property, whereby the direction of spontaneous polarization can be switched by an applied electric field. These materials are called as ferroelectrics. The relationship between the sets of dielectric,

piezoelectric, pyroelectric and ferroelectric can be simplified in the Venn diagram in Figure 2.3.

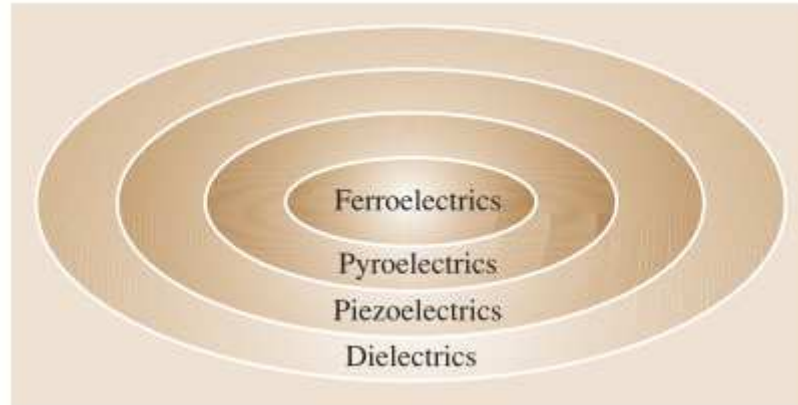


Figure 2.3: Venn diagram of subclasses of dielectric materials (Safa & Peter, 2007)

### 2.2.1 Structural origin of the ferroelectric state

Ferroelectric materials comprised of an arrangement of positive and negative direction; when an electric field,  $E$  is applied, the dipoles are induced within the structure and become align, thus exhibiting spontaneous polarization. The regions with the set of the spontaneously polarized dipoles are called domains. However, when an electric field is applied, the domains tend to polarized along the positive direction. At the sufficient electric field, the domains are polarized parallel to the applied field indicating a state of saturation ( $P_s$ ) and the material is said to be single domain. When the electric field is reduced to zero, the extent of polarization decreases, but not return to zero. This material is said to be remanent polarization ( $P_r$ ). The material reaches saturation again with all the domains polarized along the negative direction upon continuing the reversing field. This type of plot is called ferroelectric hysteresis loop which can be illustrated in Figure 2.4.

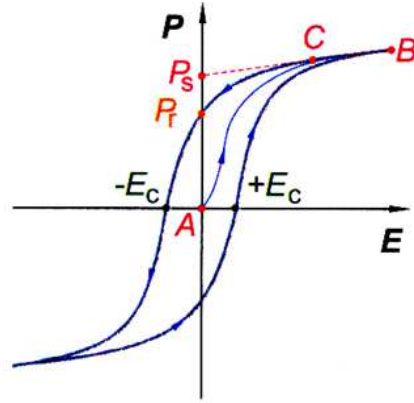


Figure 2.4: Ferroelectric hysteresis loop (Vilarinho, 2005)

### 2.3 Development of ferroelectric materials

Interesting discovery of ferroelectric, pyroelectric and piezoelectric properties was firstly discovered from inorganic compound, which is known, as Rochelle salt (sodium potassium tartrate tetrahydrate)  $\text{KNaC}_4\text{H}_4\text{O}_6 \cdot 4\text{H}_2\text{O}$  (Haertling, 1999). In the mid-1600s, it was the first discovery of ferroelectricity prepared by Elie Seignette in La Rochelle, France, for medication (Haertling, 1999). In 1824, pyroelectricity (thermal-polar) was then found. In 1880, piezoelectricity (stress-polar) was discovered. The real breakthrough of ferroelectricity was actually reported in 1924, whereby the relation between polarization and electric field was formed in the single-crystal of Rochelle salt with the presence of charges (Valasek, 1924). In the mid-1940s, the first ferroelectric ceramic material barium titanate,  $\text{BaTiO}_3$  was discovered by Hippel and his group (Randall et al., 2004). The discovery of ferroelectricity in  $\text{BaTiO}_3$  ceramics was extremely important as it demonstrated for the first time that ferroelectricity could exist in simple oxide materials.

### 2.3.1 Ferroelectric ceramic materials

In general, there are four main groups of materials have been considered which exhibit piezoelectric, pyroelectric and ferroelectric and those are hydrogen bonded systems, ionic crystals, narrow gap semiconductors and organic polymers (Vilarinho, 2005). Among them, the most important group is ionic crystals. Within this group, the main type of structure should be considered is the corner sharing oxygen octahedral, which includes the four following important families of materials (Vilarinho, 2005). These four structure types are bronze tungsten ( $A_2B_2O_6$ ), perovskite ( $ABO_3$ ), pyrochlore ( $AB_2O_7$ ) and bismuth-layer structures ( $Bi_4Ti_3O_{12}$ ) (Jardiel et al., 2008). Figure 2.5 shows the corner sharing octahedral structures. The structural arrangement with the presence of ions of small size and large charge in oxygen octahedra is favourable for the occurrence of ferroelectricity in oxides (Subbarao, 1962).

Among these, the bismuth-layer structures are particularly significant, from the point of view applications. This is because such materials generally undergo a phase transition from ferroelectric to paraelectric state at high temperature. The temperature where the phase transition occurs is called as a Curie temperature,  $T_c$  (Vilarinho, 2005). Materials with high ferroelectric transition temperature show ferroelectricity from room temperature to Curie temperature, whereas those with transition above Curie temperature exhibit an important paraelectric effect. Besides, the ability to design the physical properties required for certain applications, by formation of solid solutions, the possibility of fabrication as single crystal ceramics, textured ceramics and thin and thick films adds value to this family of materials.

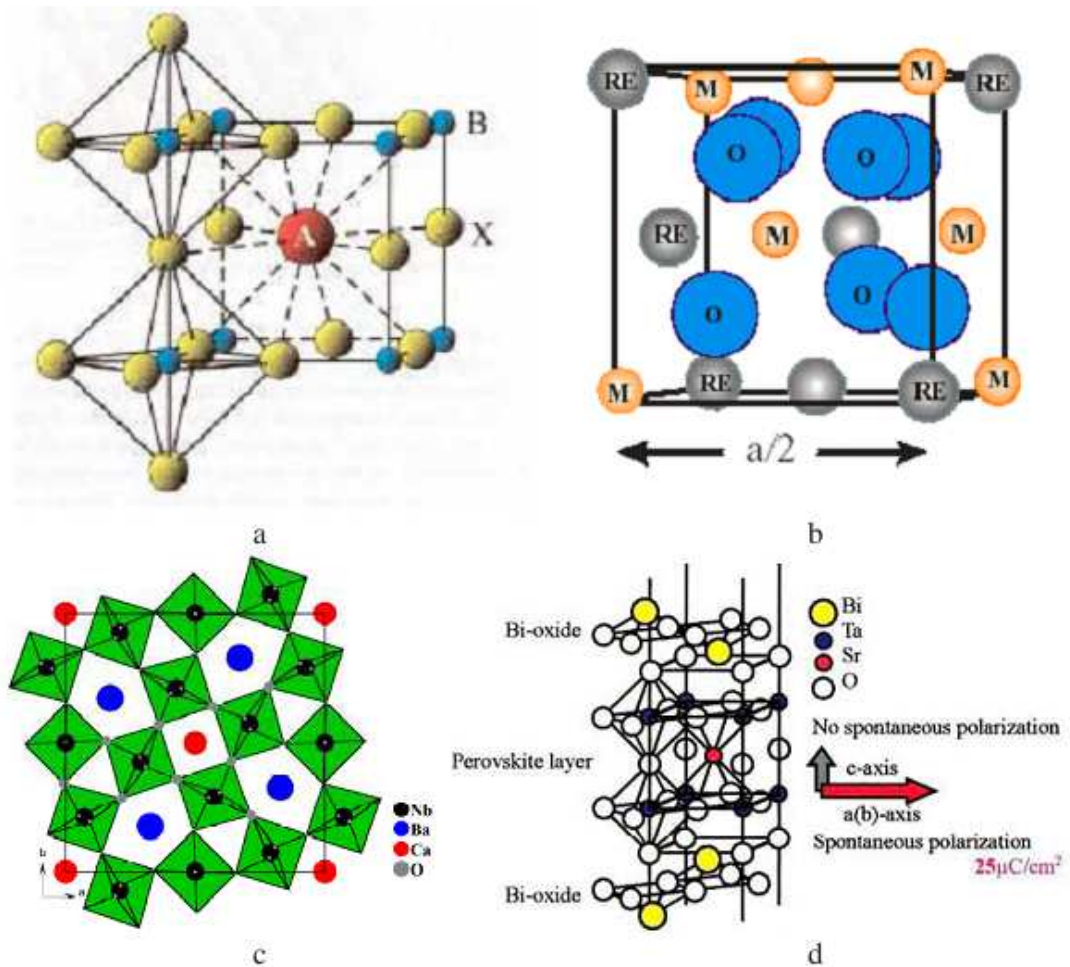


Figure 2.5: Corner sharing octahedral structures: (a) perovskite, (b) pyrochlore, (c) tungsten bronze and (d) bismuth layer (Vilarinho, 2005)

### 2.3.2 Bismuth-layer structures

Bismuth-layer structure was firstly discovered by Bengt Aurivillius in the late 1949 (Subbarao, 1961). In 1959, Smolenskii described the ferroelectricity in the  $\text{PbBi}_2\text{Nb}_2\text{O}_9$ , the first ferroelectric compound with a layer-type structure which is a member of a family of mixed bismuth oxides (Subbarao, 1961). In structure standpoint, all compounds in bismuth-layer structure can be described with the general formula,  $(\text{Bi}_2\text{O}_2)^{2+} (\text{A}_{m-1}\text{B}_m\text{O}_{3m-1})^{2-}$  where A is a mono, di or trivalent large cation (or a mixture of them) and B tri, tetra, penta or hexavalent small cation (or a mixture of them) and  $m$  are an integer named integration factor (Subbarao, 1962). To

date, more than seventy compounds have been reported in the bismuth-layer structure, and more than fifty of them are ferroelectric. In the literature, these compounds are mentioned as Aurivillius members, bismuth-based layered compounds, perovskite-based layered structures, layered bismuth oxides, layered bismuth ferroelectric compounds or other similar denominations (Jardiel et al., 2008).

## 2.4 Bismuth titanate

Bismuth titanate ( $\text{Bi}_4\text{Ti}_3\text{O}_{12}$  or BIT) is a member of bismuth based layered ferroelectric oxide that consists of the general chemical formula of  $(\text{Bi}_2\text{O}_2)^{2+}(\text{A}_{m-1}\text{B}_m\text{O}_{3m-1})^{2-}$ , where A, B and  $m$  represent  $\text{Bi}^{3+}$ ,  $\text{Ti}^{4+}$  and 3, respectively. This corresponds to the basic structure of BIT, whereby the crystal structure consists of two perovskite-like  $(\text{Bi}_2\text{Ti}_3\text{O}_{10})^{2-}$  layers sandwiched between  $(\text{Bi}_2\text{O}_2)^{2+}$  layers along the  $c$ -axis (Figure 2.6). BIT has a strong anisotropic property with the lattice constant,  $c$ -axis larger than  $a$ - and  $b$ -axes. Based on this, the lattice parameters of BIT can be written  $a = 5.4500$ ,  $b = 5.4059$  and  $c = 32.8320 \text{ \AA}$ , and  $\beta = 90.01^\circ$ .

In general, the electrical results are influenced by the strong anisotropic properties of BIT. BIT single crystal shows spontaneous polarization values of 50 and  $4 \mu\text{C}/\text{cm}^2$ , coercive field values of 50 and 60 kV/cm and dielectric constant of 160 and 130, along the  $a$ - and  $c$ -axis, respectively (Xiang et al., 2006; Kao et al., 2008b). Moreover, the Curie temperature of BIT is about  $675^\circ\text{C}$ . BIT therefore shows ferroelectric properties at room temperature. Thus, BIT materials have been intensively investigated due to its useful anisotropic properties and high Curie temperature.

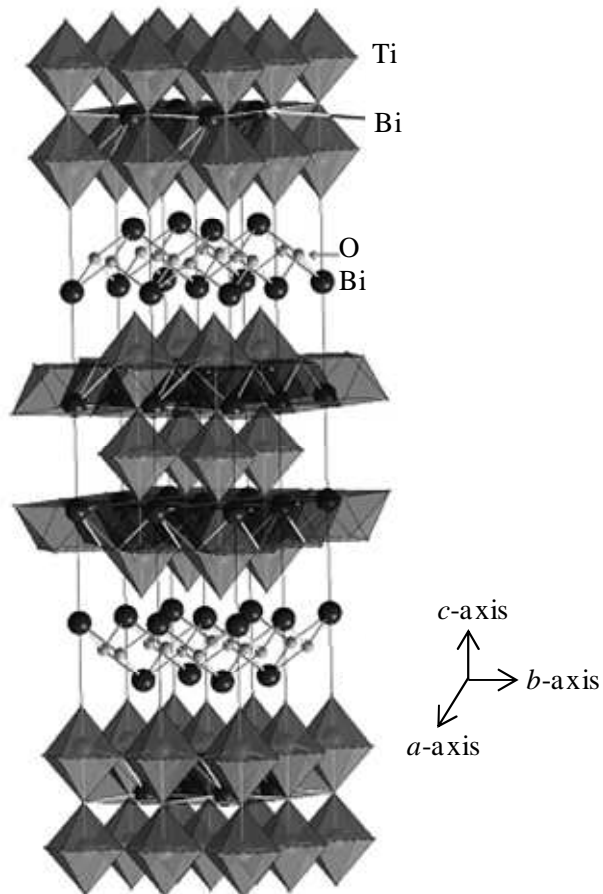


Figure 2.6: Schematic presentation of crystal structure of an Aurivillius layered BIT compound (Stojanović et al., 2008)

#### 2.4.1 Properties of BIT ceramics

In general, the properties of BIT ceramics such as powder morphology, grain microstructure and electrical properties (dielectric and ferroelectric) are highly dependent on many parameter studies. These can be simplified as the processing method, heat treatment condition and temperature, grain orientation and densification. These factors are discussed briefly as follows.

### 2.4.1.1 Powder morphology

Several works pointed out the influence of processing methods on particle morphologies are summarized in Table 2.1. Hou et al. (2010) reported that BIT nanoparticles with a narrow average particle size distribution in the range of 10 - 50 nm was synthesized via a metal-organic polymeric precursor process. Nevertheless, the formation of agglomeration was noticeable. This was attributed to Van der Waals forces due to high tendency to reduce surface free energy. Strong agglomeration of BIT powders was also produced due to high energy milling as practised in mechanical activation technique (Stojanović et al., 2006a). In precipitation method, the irregular shape with high agglomeration was observed by Pookmanee et al. (2004b). Thus, agglomeration is another challenge in the preparation of BIT powders.

Table 2.1: Particle morphologies of BIT prepared by various processing methods

Methods	Morphology	Reference
Hydrothermal synthesis	Spherical powders and 0.50 – 1.20 $\mu\text{m}$ in diameter	Pookmanee et al. (2004a)
Precipitation method	Irregular in shape, highly agglomerated, size 0.5 – 0.7 $\mu\text{m}$	Pookmanee et al. (2004b)
Mechanical activation technique	Strong agglomeration	Stojanović et al. (2006a)
Oxalate and citrate coprecipitation	Particle size less than 1 $\mu\text{m}$	Thongtem & Thongtem (2004)
Sol-gel process	Plate-like grains, average size 30 nm	Du et al. (2008)
Metal-organic polymeric precursor process	Plate-like shape	Hou et al. (2010)
Self-combustion synthesis	Plate-like shape, 10 – 20 $\mu\text{m}$	Krengvirat et al. (2011)

Several works have been done to minimize the agglomeration issue. The hydrothermal synthesis studied by Pookmanee et al. (2004a), claimed that less agglomeration was achieved with prolong reaction time from 5 to 15 hours. They succeed to produce the spherical powders in shape and well-dispersed with a range of 0.50 – 1.20  $\mu\text{m}$  in diameter (Figure 2.7). Thongtem & Thongtem (2004) studied the effectiveness of citrate and oxalate coprecipitation methods on powder morphology. The improved powder morphology was obtained by citrate method whereby the agglomeration issue was successfully minimized at calcination of 500°C. Upon increasing calcination temperature, both methods produced the powders with better dispersion.

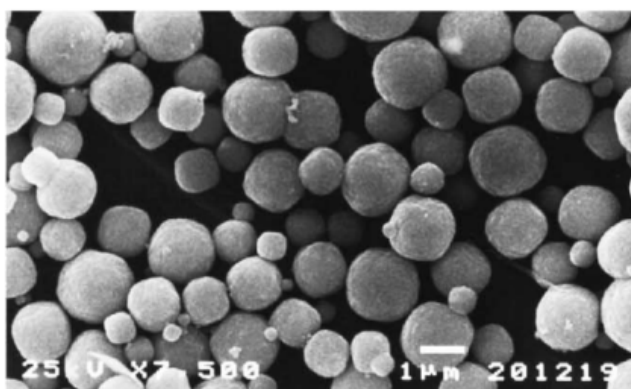


Figure 2.7: BIT powders with spherical shape and less agglomeration produced by hydrothermal route (Pookmanee et al., 2004a)

Krengvirat et al. (2011) studied the low-temperature self combustion synthesis with different pH on the BIT powders. The hard agglomeration of plate-like powders was decreased from acidic to neutral condition as shown in Figures 2.8(a) and (b), respectively. This can be explained by the explosion of Ti–OH in the precursor that contained a large amount of  $\text{H}^+$ . This led to a high content of the Ti–O<sup>-</sup> hydroxyl group, and thus resulted in strong attractive force between the particles. The addition

of the OH ions generated Ti-OH force between the particles, and thus resulted in a soft agglomeration.

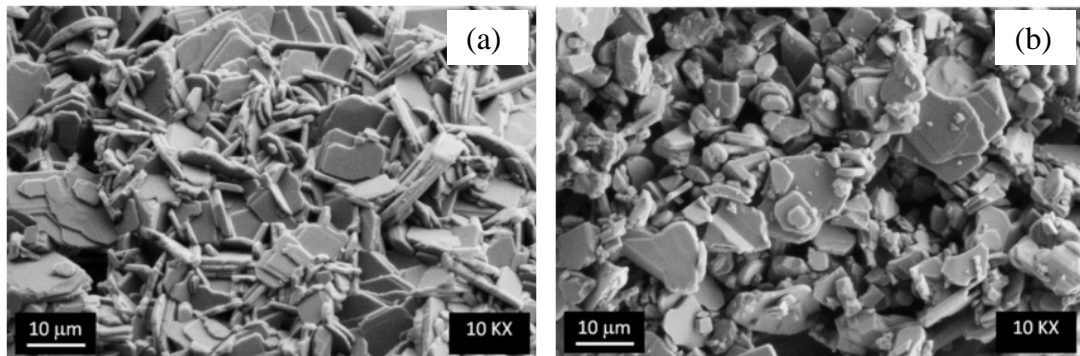


Figure 2.8: (a) hard agglomeration at pH 3 and (b) soft agglomeration at pH 7 (Krengvirat et al., 2011)

Other than that, the particle shape is highly influenced by the processing method. As seen in Figures 2.7 and 2.8, the formation of BIT powders with different particle shape was obvious. The spherical that characterized by hydrothermally powders and the platey shape by combustible powders are clearly shown, respectively. Nevertheless, Gu et al. (2008) reported that the processing method is not the core reason to produce BIT powder with different shape. They added that the other additional materials such as type of mineralizer and additive succeed to produce nanoplates, as shown in Figure 2.9. It was also supported by other work, whereby the other factors such as the mineralizer content, molar ratio of Bi:Ti, reaction time and temperature also affect the powder morphology (Shi et al., 2000).

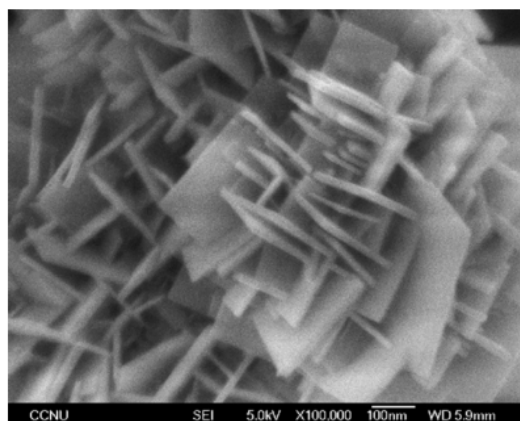


Figure 2.9: BIT nanoplates synthesized by hydrothermal method assisted PEG addition (Gu et al., 2008)

Varying calcination temperature is an essential parameter that influences the powder morphology. Du et al. (2008) reported low calcination temperature for the preparation of BIT powder via sol-gel method. They claimed that the crystallization temperature of BIT synthesized by sol-gel method occurred at 425°C and there was no evidence the presence of intermediate phase. In other work by Pookmanee (2008), the precipitated powders were calcined from 600 to 900°C for 2 hours (Figure 2.10). They reported that the particle size increased as the calcination temperature increased. The average particle size at 900°C was 300 nm.

Kan et al. (2003a) studied the molten salt synthesis method to produce BIT platelets in NaCl-KCl and Na<sub>2</sub>SO<sub>4</sub>-K<sub>2</sub>SO<sub>4</sub> fluxes. They found that the calcination temperature of BIT was influenced by homogeneity of the starting materials. It is well known that the morphology and compositional homogeneity of the powders greatly influence the calcination temperature. It was reported that calcination temperature was significantly reduced by 30 - 40% via wet chemical synthesis in comparison to the conventional solid state reaction (Hou et al., 2010; Zhi-hui et al., 2010).

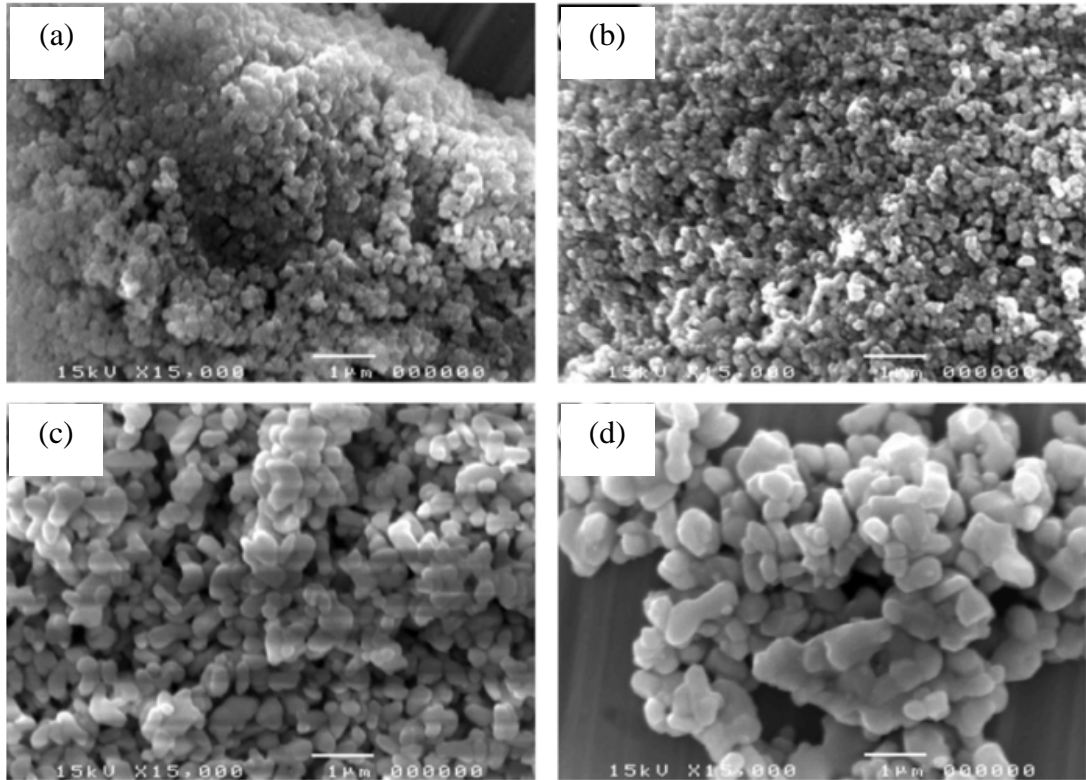


Figure 2.10: SEM micrographs of BIT powders calcined for 2 h at (a) 600, 700, 800 and 900°C (Pookmanee, 2008)

#### 2.4.1.2 Grain microstructures

The main morphology of BIT powders is generally ascribed as plate-like structure. It is also known that BIT has highly anisotropic properties, whereby it is electrical dependent. For instance, BIT single crystals show bi-axial polarization. Along the a-axis, the spontaneous polarization can achieve up to  $50 \mu\text{C}/\text{cm}^2$ , while that along the c-axis does not exceed  $4 \mu\text{C}/\text{cm}^2$  (Noguchi et al., 2008). Taking this into account, the main concern on microstructural is not only involved on porosity and grain size, but also orientation in a polycrystalline ceramic.

Nowadays, many attempts have been carried out to enhance the grain orientation which in turn to improve the electrical properties. Chen et al. (2006a) reported that the orientation of BIT grains could be prepared by magnetic alignment,

as shown in Figure 2.11. They also added that the magnetic alignment was found to be an effective technique to prepare highly *a-b* plane-oriented BIT ceramics with the enhancement of dielectric properties. Earlier than that, Makiya et al. (2003) reported that particle oriented BIT ceramics with high density was developed by a high magnetic field. There are also several reports that the plate-like particle of BIT could be oriented by hot forging, tape casting and template grain growth (Horn et al., 1999; Seth & Schulze, 1989). However, the preparation using magnetic alignment has outstanding merits such as easily and freely to control the direction of orientation and magnetic field (Tanaka et al., 2009).

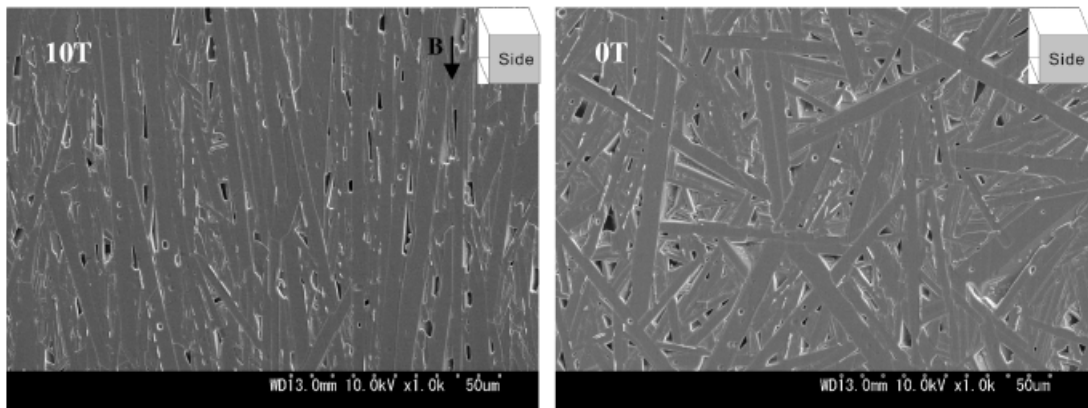


Figure 2.11: SEM of thermally etched surfaces of sintered BIT samples with (10T) and without (0T) magnetic alignment (Chen et al., 2006a)

#### 2.4.1.3 Dielectric and ferroelectric properties

BIT is known to have several outstanding dielectric and ferroelectric properties. The performance of both properties is strongly dependent on several factors, i.e. inherent defects, sintering temperature, types of sintering, grain orientation and synthesis route. Noguchi et al. (2000) reported that the ferroelectric properties of BIT were suppressed by domain pinning due to inherent defects such as bismuth vacancies ( $V_{Bi}^{\prime\prime\prime}$ ) and oxygen vacancies ( $V_O^{\prime\prime}$ ). They also concluded that the high leakage current of BIT that associated with bismuth and oxygen vacancies was

significantly improved by small addition of Bi excess instead of low annealing temperature in air.

Kong et al. (2001) studied the ferroelectric properties at different sintering temperatures. They claimed that the ferroelectric properties are strongly influenced by sintering temperature, whereby the remanent polarization was suddenly decreased at higher sintering temperature due to volatility effect. Macedo et al. (2004b) investigated the dielectric and ferroelectric properties using CO<sub>2</sub> laser sintering process. They found out that higher space charge concentration was reduced at high laser power intensity in order to give a great improvement in dielectric and ferroelectric properties. In other work by Chen et al. (2006a), they reported that the improved dielectric constant was achieved when the grain texture was aligned by magnetic field. In their work, the dielectric constant in the parallel direction was recorded of about 15000 while 5000 in the perpendicular and random at 500°C (Figure 2.12).

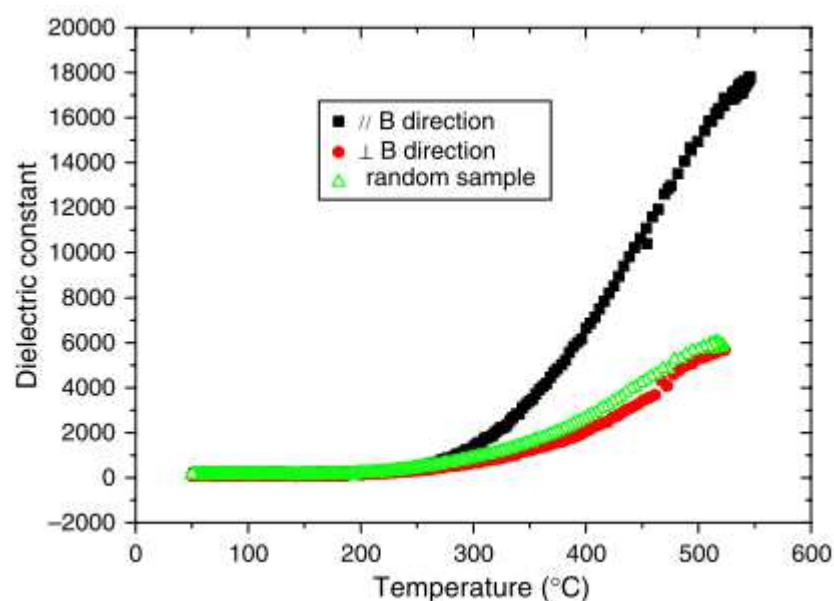


Figure 2.12: Dielectric constant of BIT ceramics measured at different direction (Chen et al., 2006a)